analytical chemistry

pubs.acs.org/ac Article

Integrating-Sphere-Assisted Resonance Synchronous Spectroscopy for the Quantification of Material Double-Beam UV−Vis Absorption and Scattering Extinction

Max Wamsley,[§] Pathum Wathudura,[§] Juan Hu, and Dongmao Zhang*

Cite This: *Anal. Chem.* 2022, 94, 11610−11618 Read Online

ACCESS | Metrics & More | Article Recommendations | Supporting Information

ABSTRACT: Integrating spheres (IS) have been used extensively for the characterization of light absorption in turbid samples. However, converting the IS-based sample absorption coefficient to the UV−vis absorbance quantified with a double-beam UV−vis spectrophotometer is challenging. Herein, we report an integrating-sphere-assisted resonance synchronous (ISARS) spectroscopy method performed with conventional spectrofluorometers equipped with an integrating-sphere accessory. Mathematical models and experimental procedures for quantifying the sample, solvent, and instrument-baseline ISARS intensity spectra were provided. A three-parameter analytical model has been developed for correlating the ISARS-based UV−vis absorbance and the absorbance measured with double-beam instruments. This ISARS method enables the quantitative separation of light absorption and scattering contribution to the sample UV−vis extinction spectrum measured with double-beam UV−vis spectrophotometers. Example applications of this ISARS technique are demonstrated with a series of representative samples differing significantly in their optical complexities, from approximately pure absorbers, pure scatterers, to simultaneous light absorbers, scatterers, and emitters under resonance excitation and detection conditions.

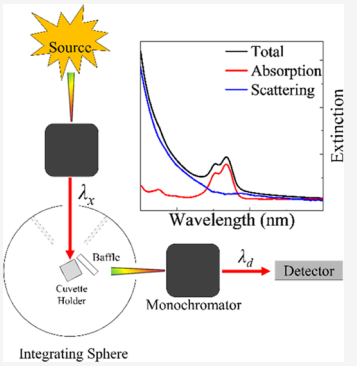

INTRODUCTION

UV−vis spectrophotometry is the most used method in chemical, biological, and materials sciences for its high reproducibility and affordability.[1−4] However, quantitative decoupling of the light scattering and absorption contribution to the sample UV−vis extinction spectrum can be challenging for materials that cannot be approximated as pure light absorbers or scatterers. While the default unit of the UV−vis signal obtained with commercial UV−vis spectrophotometers is, to the best of our knowledge, invariably absorbance (the absorption extinction), what is quantified with these instruments is the light extinction, the sum of the material absorption and scattering extinctions. Unfortunately, this often leads to spectral misinterpretation. It has remained a persistent and prevalent literature practice to directly take the UV−vis extinction spectra as the absorbance spectra even for nanoparticle samples that likely have a significant scattering extinction.[2,3,5−8]

Light scattering is a universal material property due to the nonzero polarizability of all matter. For dissolved small molecular chromophores, however, the scattering contribution to the sample UV−vis extinction is negligible because the scattering coefficients of these samples are usually drastically smaller than their absorption coefficients. For macromolecules, supramolecules, and nanoscale materials, the scattering contribution to the sample extinction UV−vis can be significant.[9−11] Reliable quantification of the scattering and absorption activities is critical for material design and applications because scattering and absorption differ fundamentally in their causes and effects. Absorbed photons can trigger photoelectron generations in photovoltaic applications,[12,13] photoluminescent emissions in fluorescence sensing, singlet oxygen generations in photodynamic therapy,[14] and chemical reactions in photocatalysis.[15] On the other hand, materials with high scattering activity can be used for applications such as intracellular imaging and UV light blocker for sunscreen. Separating material light absorption and scattering contribution to their UV−vis spectra is also necessary for reliable chemical measurements. As an example, it has been recently shown that only light absorption causes the sample inner filter effect on the fluorescence signal, while scattering with an extinction as large as 1 has no significant effect on the fluorescence signal.[16]

Several approaches have been explored for decomposing UV−vis extinction spectra of solutions into their absorbance and scattering extinction spectra.[17−21] However, the applicability and accessibility of those methods to general samples are limited. As examples, the method developed by Lin simultaneously measured the transmitted and 90° propagated

Received: May 10, 2022
Accepted: August 2, 2022
Published: August 12, 2022

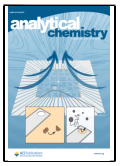

https://doi.org/10.1021/acs.analchem.2c02037
Anal. Chem. 2022, 94, 11610−11618

photons using a home-developed fiber-coupled spectrometer[18] and subsequently deduced the light absorption and scattering extinction. However, this method is applicable only to nonfluorescent samples. Further, neither the sample inner filter effect on light scattering induced by the light absorption nor the effect of light scattering depolarization on the signal detection has been considered. The resonance synchronous spectroscopic approach considered the interplay among the sample absorption and scattering, but the effect of scattering depolarization (or anisotropy) and sample on-resonance fluorescence has not been considered.[17]

Integrating spheres (IS) have long been applied for selectively quantifying the light absorption of turbid solutions and solid materials even for single particles. These measurements were performed mostly with home-built IS-equipped spectrophotometers with the sample cuvette placed inside the IS.[22−28] Unlike the double-beam UV−vis absorbance that allows the quantification of materials' molar absorptivity, which is an intrinsic material property, the IS-based UV−vis absorbance is instrument-specific. The latter depends not only on the sample absorptivity and concentration but also on the geometry and optical characteristics of the IS such as the reflectivity and absorptivity of the surface coating, the cuvette sizes, and sample volumes. Such instrument dependence explains why wavelength-dependent IS-assisted absorbance is commonly referred to as the absorptivity coefficient spectrum and not as the absorbance spectrum acquired with double-beam instruments. For convenience, we refer to the absorption spectra obtained with both IS-based and double-beam instruments as the absorbance spectra

$$A_{IS}(\lambda) = aA_{db}(\lambda) \quad (1)$$

$$A_{IS}(\lambda) = a(A_{db}(\lambda))^2 + bA_{db}(\lambda) \quad (2)$$

Theoretical or empirical mathematical models such as those shown in eqs 1 and 2 have been developed for converting the IS-derived absorbance $A_{IS}(\lambda)$ and double-beam UV−vis absorbance $A_{db}(\lambda)$ spectrum.[24−28] Most of the theoretical models are developed by assuming that the inner coating layer of the IS is a perfect diffuse reflector with no absorbance, while the empirical models are generated by curve-fitting IS-based UV−vis absorbance as a function of the double-beam absorbance in a series of chromogenic sample of different concentrations. Further, the existing IS-based absorbance quantification is performed mostly with UV−vis spectrophotometer or similar instruments equipped with an excitation monochromator but with no detection monochromator.[22,24,25,27−33] These approaches are susceptible to fluorescence and Raman interferences that can be from the sample, solvents, and the integrating sphere itself (*vide infra*). The fluorescence and Raman interference is negligible in the double-beam UV−vis measurements because of the spatial selectivity of the detector in the spectrophotometer, i.e., only the photons propagated along the incident light can interfere with the UV−vis spectrophotometric quantification of the transmitted light. However, fluorescence emission and Raman signal triggered inside and by the IS inevitably lead to underestimated IS-based absorbance when a spectrophotometer is used as the detector. The latter occurs due to the IS capturing all fluorescence and Raman photons with no spatial selectivity.

IS-equipped UV−vis spectrophotometers are also commercially available. These instruments, including the one used in this work (Figure 1B), are usually configured such that the sample is placed outside the integrating sphere, whereas home-built IS-equipped spectrophotometers usually have the cuvettes placed inside the IS (Figure 1A).[24−28] The configuration adopted by these commercial spectrophotometers reduces the fluorescence interference because only the forward propagating fluorescence photons can lead to falsely low absorbance extinction. However, it will drastically enhance the susceptibility to the scattering interference because this configuration captures only the forwardly propagated scattering photons in the absorbance determination. As a result, the scattered photons propagated in the other directions lead to overestimated sample absorbance, which will be shown in the experimental data (*vide infra*).

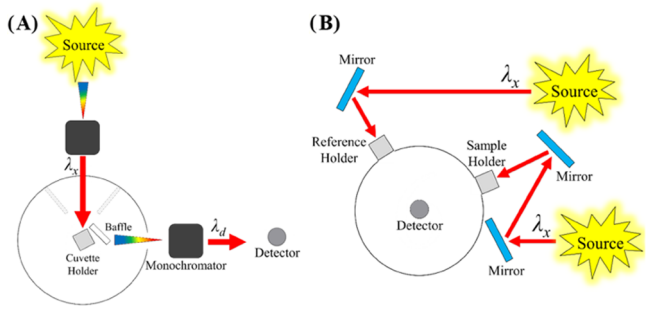

Figure 1. (A) Scheme of the ISARS spectral acquisition performed with a commercial spectrofluorometer. The excitation and detection wavelength are kept the same (*resonance*) and varied simultaneously (*synchronous*) during the ISARS data acquisition. (B) Sampling scheme of the commercial IS-equipped UV−vis spectrophotometer used in this work.

Herein, we report an IS-assisted resonance synchronous (ISARS) spectroscopic method and its applications for the quantification of UV−vis absorbance for samples from approximately pure absorbers, pure scatterers, to simultaneous light absorbers, scatterers, and emitters under the resonance excitation and detection conditions. Two three-parameter analytical models are developed, one for predicting the ISARS spectral intensity as a function of the sample double-beam UV−vis absorbance and the other for correlating the ISARS-based absorbance and the double-beam UV−vis absorbance. This ISARS technique is broadly accessible because it is implemented with a commercial spectrofluorometer (Figure 1) and IS accessory. These spectrofluorometers and IS accessories have been commonly used for fluorescence quantum yield measurements.[28,34−37]

ISARS spectra are acquired wavelength by wavelength under resonance excitation and detection conditions ($\lambda_x = \lambda_d$), crossing the entire wavelength region. In this case, only the "on-resonance" detected fluorescence photons interfere with the ISARS-based absorbance quantification. It is important to note that such "on-resonance" detected fluorescence usually contains anti-Stokes-shifted fluorescence (ASSF), on-resonance fluorescence (ORF), and Stokes-shifted fluorescence (SSF). Such a complexity arises from the fact that both excitation and detection monochromators have finite bandwidths. Besides ORF, an off-resonance signal including ASSF and SSF also contributes to the fluorescence detected under resonance excitation and detection conditions.[19,38,39] ORF refers to the fluorescence emission at the excitation wavelength. While the ORF theory has been depicted in Jablonski's

https://doi.org/10.1021/acs.analchem.2c02037
Anal. Chem. 2022, 94, 11610−11618

energy diagram for decades,[40] it has been commonly mistaken as light scattering in the current spectral analysis.

Theoretical Consideration. The analytical models for describing ISARS intensity and ISARS-based absorbance as a function of the sample double-beam absorbance are developed for samples that can be approximated as pure light absorbers with no light scattering and on-resonance fluorescence. The impacts of the fluorescence and light scattering on the ISARS-based UV−vis absorbance quantification will be evaluated empirically in the Results and Discussion section.

ISARS Spectrum. Photons that entered the IS undergo one of the following three processes before or after each diffusion reflection: (1) being absorbed by the sample or IS itself, (2) exiting the IS through the excitation or detection ports, (3) continuing diffuse reflections inside the IS until all incident photons are absorbed by the sample, IS, or escape the IS through the excitation and detection ports. Only a small fraction of the photons exiting the IS through the detection port can contribute to the ISARS spectrum. The ISARS spectral intensity is the sum of a series of stepwise ISARS signals defined by the number of diffuse reflections by the photons before all incident photons are depleted from the IS. This stepwise ISARS intensity can be modeled as a function of the following parameters:

(1) The multiplication product of concentration (C) and molar absorptivity $\varepsilon(\lambda)$ or the sample double-beam absorbance $A_{db}(\lambda)$ that is assumed to be acquired with a 1 cm UV−vis cuvette.
(2) The fraction of the excitation port $\eta_x(\lambda)$ and the detection port $\eta_d(\lambda)$ through which the photon can exit the IS after each diffuse reflection.
(3) The effective sample absorption pathlength $r(\lambda)$ associated with each pass of the photons inside the IS through the sample. It is noted that $r(\lambda)$ is actually a pathlength ratio between the effective sample pathlength inside the IS versus the cuvette pathlength used for the $A_{db}(\lambda)$ measurements. This unitless $r(\lambda)$ value can be viewed as the pathlength in cm since the $A_{db}(\lambda)$ is defined as the double-beam absorbance measured with a 1 cm cuvette.
(4) The UV−vis absorbance $A_s(\lambda)$ by the IS itself.
(5) A collective instrument and experimental parameter $I_0(\lambda)$ that is the multiplication product of excitation intensity, instrument photon collection efficiency, and detector responses.

Considering that only the light exiting the IS from the detection port contributes to the ISARS signal, we derived a general formula for the stepwise ISARS signal (eq 3) and the total sample ISARS signal (eq 4). Since the right-hand side of eq 4 is a power series of $I_0(\lambda)10^{-(A_{db}(\lambda)r(\lambda)+A_s(\lambda))}(1-\eta_x(\lambda)-\eta_d(\lambda))$, a simple analytical equation is derived for ISARS spectrum (eq 4). A detailed stepwise derivation of eqs 3−5 is shown in the Supporting Information.

$$I_n^{ISARS}(\lambda) = \eta_d(\lambda) I_0(\lambda) 10^{-n(A_{db}(\lambda)r(\lambda)+A_s(\lambda))} (1-\eta_x(\lambda)-\eta_d(\lambda))^{n-1} \quad (3)$$

$$I_{sample}^{ISARS}(\lambda) = \sum_{i=1}^{\infty} \eta_d(\lambda)\left(I_0(\lambda) 10^{-i(A_{db}(\lambda)r(\lambda)+A_s(\lambda))} (1-\eta_x(\lambda)-\eta_d(\lambda))^{i-1} \right) \quad (4)$$

$$I_{sample}^{ISARS}(\lambda) = I_0(\lambda) \frac{\eta_d(\lambda)\, 10^{-(A_{db}(\lambda)r(\lambda)+A_s(\lambda))}}{1-10^{-(A_{db}(\lambda)r(\lambda)+A_s(\lambda))}(1-\eta_x(\lambda)-\eta_d(\lambda))} \quad (5)$$

Equation 3 shows that the ISARS intensity of strongly light absorbing samples ($C\varepsilon(\lambda)b(\lambda) \gg 1$) should be zero. In practice, however, there is always a nonzero baseline ISARS spectrum even with saturated molecular chromophores with very high optical density (>6, for example). Such a baseline spectrum is due most likely to the inevitable instrument stray light and detector dark current. Therefore, a realistic model for the experimental sample ISARS intensity should be the sum of the sample ISARS spectrum and the baseline ISARS spectrum $I_B(\lambda)$ (eq 6).

$$I_{sample}^{ISARS,obsd}(\lambda) = I_B(\lambda) + I_0(\lambda) \frac{\eta_d(\lambda) 10^{-(A_{db}(\lambda)r(\lambda)+A_s(\lambda))}}{1-10^{-(A_{db}(\lambda)r(\lambda)+A_s(\lambda))}(1-\eta_x(\lambda)-\eta_d(\lambda))} \quad (6)$$

Experimental quantification of the baseline spectrum is straightforward by using a series of strongly light absorbing samples (*vide infra*). Equation 6 is reduced to eq 7. For these baseline evaluation samples.

$$I_{BL}^{ISARS,obsd}(\lambda) = I_B^{ISARS}(\lambda) \quad (7)$$

Equation 6 also allows one to deduce the analytical model for the solvent ISARS spectrum (eq 8) by setting $\varepsilon(\lambda)$ in eq 6 to zero.

$$I_{solvent}^{ISARS,obsd}(\lambda) = I_B^{ISARS}(\lambda) + I_0(\lambda) \frac{\eta_d(\lambda) 10^{-A_s(\lambda)}}{1-10^{-A_s(\lambda)}(1-\eta_x(\lambda)-\eta_d(\lambda))} \quad (8)$$

Correlation between $A_{db}(\lambda)$ and $A_{ISARS}(\lambda)$. $A_{db}(\lambda)$ and $A_{ISARS}(\lambda)$ refer to the UV−vis absorbance measured with the conventional UV−vis spectrophotometer and ISARS technique, respectively. Mathematically, $A_{ISARS}(\lambda)$ is defined with eq 9.

$$A_{ISARS}(\lambda) = -\log\left(\frac{I_{sample}^{ISARS}(\lambda)}{I_{solvent}^{ISARS}(\lambda)}\right) \quad (9)$$

The sample $A_{ISARS}(\lambda)$ spectra are quantified using the experimental $I_{sample}^{ISARS,obsd}(\lambda)$, $I_{solvent}^{ISARS,obsd}(\lambda)$, and $I_B(\lambda)$ spectra (eq 10).

$$A_{ISARS}(\lambda) = -\log\left(\frac{I_{sample}^{ISARS,obsd}(\lambda) - I_B^{ISARS}(\lambda)}{I_{solvent}^{ISARS,obsd}(\lambda) - I_B^{ISARS}(\lambda)}\right) \quad (10)$$

Replacing the $I_{sample}^{ISARS,obsd}(\lambda)$ and $I_{solvent}^{ISARS,obsd}(\lambda)$ defined with eqs 6 and 8 into eq 10 leads to eq 11, a first-principle model for correlating the $A_{db}(\lambda)$ and $A_{ISARS}(\lambda)$. Combining the excitation and detection port fractions leads to eq 12, which is a three-parameter model for the correlation between $A_{db}(\lambda)$ and $A_{ISARS}(\lambda)$. $f(\lambda)$ in eq 12 is the sum of $\eta_x(\lambda)$ and $\eta_d(\lambda)$, the total port fraction.

$$A_{ISARS}(\lambda) = A_{db}(\lambda) + r(\lambda) + \log\left(\frac{1-10^{-(A_{db}(\lambda)r(\lambda)+A_s(\lambda))}(1-\eta_x(\lambda)-\eta_d(\lambda))}{1-10^{-A_s(\lambda)}(1-\eta_x(\lambda)-\eta_d(\lambda))}\right) \quad (11)$$

https://doi.org/10.1021/acs.analchem.2c02037
Anal. Chem. 2022, 94, 11610−11618

$$A_{\mathrm{ISARS}}(\lambda) = A_{\mathrm{db}}(\lambda) + r(\lambda) + \log\left(\frac{1 - 10^{-(A_{\mathrm{db}}(\lambda)r(\lambda)+A_{\mathrm{s}}(\lambda))}(1 - f(\lambda))}{1 - 10^{-A_{\mathrm{s}}(\lambda)}(1 - f(\lambda))}\right) \quad (12)$$

Equation 12 has been to the best of our knowledge the first-principle-analytical model that takes into consideration the absorbance by the IS itself. This model showed that $A_{\mathrm{ISARS}}(\lambda)$ is nonlinearly correlated to $A_{\mathrm{db}}(\lambda)$. Furthermore, using calibration samples, one can quantify $r(\lambda)$, stepwise light absorption pathlength of the cuvette inside the IS, $f(\lambda)$ port fraction of the IS, and $A_{\mathrm{s}}(\lambda)$, the absorbance by the IS with the nonlinear fitting of the experimental $A_{\mathrm{ISARS}}(\lambda)$ as a function of $A_{\mathrm{db}}(\lambda)$.

MATERIALS AND METHODS

Chemicals and Equipment. $Cu(NO_3)_2$, $KMnO_4$, $NiSO_4$, and Rhodamine 6G were obtained from Sigma-Aldrich and used as received. Ultrapure $BaSO_4$ was obtained from Nacalai teque (Tokyo, Japan, Lot#M9P7734). The COOH-functionalized CdTe core-type quantum dots were purchased from Sigma-Aldrich (Lot#MKBZ9296V). The polystyrene NPs (PSNPs, Cat#21753-15) and fluorescent polystyrene NPs (fPSNPs, Cat#18719) with a diameter of 0.38 and 0.01 μm, respectively, were purchased from Polysciences Inc. Nanopure water (18.2 MΩ cm^{-1}, Thermo Scientific) was used in all sample preparations. All spectra were obtained at room temperature in a 1 cm square fused quartz UV−vis or fluorescence cuvette.

UV−Vis and ISARS Spectral Acquisition. UV−vis extinction and absorbance spectra were taken with a Shimadzu UV-2600i spectrophotometer with an ISR-2600 integrating-sphere accessory (Duisburg, Germany). ISARS spectra were obtained using a Fluoromax-4 spectrophotometer (Horiba Jobin Yvon, Edison, NJ) equipped with a K-Sphere Petite integrating sphere (Horiba PTI) with an internal diameter of 80 mm. A neutral density filter with an optical density of 2.0 ± 0.05 from 200 to 1100 nm (Thor Labs) was also used for all ISARS spectra. Unless specified otherwise, all ISARS spectra were acquired with an integration time of 0.3 s and a bandwidth of 2 nm for both excitation and emission monochromators. The spectral intensity was the ratio between the signal from the sample detector and reference detector (S1/R1).

RESULTS AND DISCUSSION

Baseline Quantification. As discussed in the Theoretical Consideration section, the ISARS baseline spectrum $I_{\mathrm{B}}^{\mathrm{ISARS}}(\lambda)$ can be determined with strongly light absorbing samples. An ideal baseline evaluation sample should have intense absorption in the entire wavelength range (300−800 nm). However, it is difficult for one sample to have sufficient absorptivity over such a broad wavelength region. Among a series of molecular chromophores we explored, $KMnO_4$, $Cu(NO_3)_2$, and $NiSO_4$ allow us to determine and cross-validate the baseline across the entire wavelength region.

Empty IS, IS with the empty cuvette, and the IS with a water-containing cuvette all give very similar ISARS spectra (Figure 2A), indicating that the quartz cuvette used in this work has negligible light absorption, and the specular reflection by the cuvette has no significant impact on the ISARS intensity. Otherwise, the ISARS spectrum obtained using the IS with and without the cuvette should be significantly different (Figure 2).

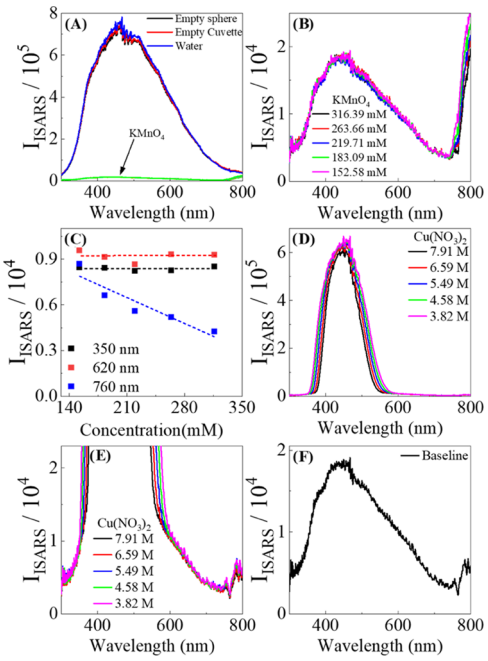

Figure 2. (A) ISARS spectra of empty IS, cuvette with water, and cuvette with $KMnO_4$ of indicated concentrations. (B) Zoom-in ISARS spectra of $KMnO_4$. (C) ISARS intensity as a function of $KMnO_4$ at three representative wavelengths. (D, E) ISARS spectra of $Cu(NO_3)_2$ indicated concentrations. (F) ISRAS baseline spectrum determined with saturated $KMnO_4$ and $Cu(NO_3)_2$.

The ISARS baseline spectrum was determined using saturated and near-saturated $KMnO_4$, $Cu(NO_3)_2$, and $NiSO_4$ solutions. Experimental identification of the workable wavelength region of these chromophores was performed using a sample dilution method. Only the ISARS signal that is independent of the chromophore concentration is taken as the baseline intensity at the probe wavelength. $KMnO_4$ alone enables baseline quantification from 300 to 750 nm (Figure 2A−C). $Cu(NO_3)_2$ allows the baseline quantification from 300 to 370 nm and 750 to 800 nm (Figure 2D−F). The workable wavelength region of $NiSO_4$ is from 330 to 450 nm and 600 to 800 nm (Figure S1). The high similarity in the baseline ISARS spectra obtained with $KMnO_4$, $Cu(NO_3)_2$, and $NiSO_4$ in their commonly workable wavelength regions provided a cross-validation of this baseline quantification method (Figure S1).

Sample volume is critical for reliable baseline spectrum determination (Figure S2). Take the baseline evaluation using saturated $KMnO_4$ as an example, a constant baseline spectrum (within the measurement error) is acquired when the sample volume is 2.5 mL or above. However, the ISARS intensity monotonically increases when the volume of the $KMnO_4$ solution in the cuvette is reduced to 2 mL. This observation is not surprising because $r(\lambda)$ decreases with the reduced volume in the cuvette. When $r(\lambda)$ is smaller than a certain threshold value, the term $10^{-(A_{\mathrm{db}}(\lambda)r(\lambda)+A_{\mathrm{s}}(\lambda))}$ in eq 6 cannot be reduced $10^{-A_{\mathrm{s}}(\lambda)}$ in eq 7 for the baseline spectral acquisition (eq 7). To ensure the reliability of our baseline correction, we use the sample volume of 3 mL in all of the subsequent measurements.

Correlation between $A_{\mathrm{db}}(\lambda)$ and $A_{\mathrm{ISARS}}(\lambda)$. The validity of the analytical model (eq 12) for correlating the samples

https://doi.org/10.1021/acs.analchem.2c02037
Anal. Chem. 2022, 94, 11610−11618

$A_{db}(\lambda)$ and $A_{ISARS}(\lambda)$ was evaluated using $KMnO_4$ and $NiSO_4$ as the two chromophores absorbing collectively across the entire wavelength from 300 to 800 nm. The data obtained with $KMnO_4$ is shown in Figure 3 and that for $NiSO_4$ is shown in

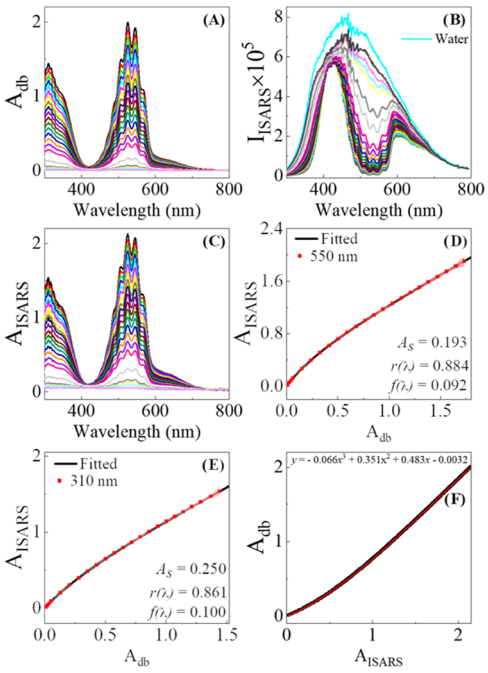

Figure 3. (A) Double-beam UV−vis spectra $A_{db}(\lambda)$ of the $KMnO_4$ solutions at different concentrations. (B) Baseline-corrected ISARS spectra of water and $KMnO_4$ solutions. (C) ISARS-derived UV−vis absorbance spectra $A_{ISARS}(\lambda)$ of the $KMnO_4$ solutions using eq 10. (D, E) (Dots) Experimental and (solid line) curve-fitting correlation between $A_{db}(\lambda)$ and $A_{ISARS}(\lambda)$ for two representative wavelengths. The standard deviation of $A_{ISARS}(\lambda)$ is shown by the shaded region. (F) An example third-order polynomial fitting of the $A_{db}(\lambda)$ intensity as a function of $A_{ISARS}(\lambda)$. The fitted data is generated with eq 12 using the $A_s(\lambda)$, $r(\lambda)$, and $f(\lambda)$ values shown in plot (D) and with the $A_{db}(\lambda)$ varying from 0.01 to 2.5 with a step value of 0.01.

the Supporting Information (Figures S3 and S4). The $A_{ISARS}(\lambda)$ values (Figure 3C) are calculated using eq 10 and the baseline-corrected ISARS spectra (Figure 3B) obtained with the solvent and the $KMnO_4$ solutions. The $A_{db}(\lambda)$ and $A_{ISARS}(\lambda)$ are nonlinearly correlated with each other, which is consistent with the theoretical model derived in this work (eq 12). Fitting the experimental $A_{ISARS}(\lambda)$ values of $KMnO_4$ and $NiSO_4$ as a function of their respective $A_{db}(\lambda)$ with the three-parameter model (eq 12) enables us to quantify $A_s(\lambda)$, the IS absorbance; $r(\lambda)$, the effective photon pathlength through the cuvette inside the IS after each diffuse reflection; and $f(\lambda)$, the port fraction as a function of the excitation wavelength (Figure S5). The samples used for curve-fitting determination of the $A_s(\lambda)$, $r(\lambda)$, and $f(\lambda)$ values all have a double-beam absorbance of 0.05 or higher at the evaluated wavelength. The fitting errors with the determined $A_s(\lambda)$, $r(\lambda)$, and $f(\lambda)$ values are all negligibly small (Figures 3D,E, S3, and S4). Equal importantly, the $A_s(\lambda)$, $r(\lambda)$, and $f(\lambda)$ values obtained by curve-fitting the $KMnO_4$ and $NiSO_4$ in their overlapping wavelength region are all in good agreement, indicating that $A_s(\lambda)$, $r(\lambda)$, and $f(\lambda)$ are sample-independent parameters.

The $r(\lambda)$ values are 0.85 ± 0.03 cm across the wavelength region, which is smaller than the physical pathlength of the 1 cm square cuvette used in this work. This result is not surprising because after each diffuse reflection, only a small fraction of photons can go through the samples inside the IS, and the stepwise pathlength is an average of the photons both passing and bypassing the sample after each diffuse reflection. The $f(\lambda)$ values in the 300−660 nm region are 0.05 ± 0.03. Such a port fraction is significantly higher than 0.008, the port area fraction of the IS used in this work. This discrepancy strongly suggests that the probability of photons exiting from the excitation and detection port depends not only on the physical port fraction but also on the internal IS configuration and the light scattering depolarization by the IS. The commercial IS used in this work has three baffles schematically shown in Figure 1. These baffles likely enhanced the photon escape from the excitation and/or detection ports. Further testing this hypothesis is currently impossible as it requires custom-made IS with different configurations.

The average $A_s(\lambda)$ value is 0.2 ± 0.08 in the wavelength region from 300 to 800 nm, which is significantly higher than the reflectance (>96−99%) specified by the IS vendor. The absorbance is especially large in the wavelength region below 350 nm. One likely reason is the chemical contamination in the inner IS coating layer that can occur during the IS fabrication and IS usages. This hypothesis is supported by the fact that exceedingly strong background IS fluorescence is shown in the background fluorescence spectrum obtained with the empty cuvette and cuvette with water, both with and without the IS (Figure S6), and the fluorescence spectrum obtained with ultrapure barium sulfate powder (Figure S7), which is one of the most used IS coating materials for its high reflectivity. Without the IS fluorescence impurities (thereby absorption impurity because light absorption must proceed photoluminescence), one would expect fluorescence spectra obtained with the empty cuvette and water-containing cuvette inside the IS to be approximately the same as their respective counterparts acquired without the IS. Such a strong IS background fluorescence interference is surprising because the IS employed in this work has been used for less than 1 year and exhibits no visual contamination.

The strong Raman and fluorescence background interference from the IS itself also highlight the difficulty in using a UV−vis spectrophotometer as a detector for the IS-based quantification. The spectra obtained with double-beam UV−vis spectrophotometers equipped with an IS accessory can be viewed as ISARS with an infinitely large detection wavelength bandwidth since there is no detection monochromator. In this case, any IS background fluorescence and Raman scattering will affect IS-based absorbance quantification. In contrast, with the spectrofluorometer-based ISARS developed in this work, one can minimize IS fluorescence and Raman interference by controlling the detection monochromator bandwidth, while the IS absorption interference is included in the mathematic model (eq 12).

Prediction $A_{db}^{ISARS}(\lambda)$ Using Experiment $A_{ISARS}(\lambda)$. Besides providing the mechanistic quantitative understanding of the correlation between the ISARS-based absorbance and double-beam absorbance, the analytical model (eq 12) also provides a basis for converting the sample instrument-dependent ISARS-based absorbance to its instrument-independent double-beam absorbance. Even though it is straightforward to use eq 12 to calculate the sample ISARS-based UV−vis absorbance $A_{ISARS}(\lambda)$ from its double-beam UV−vis absorbance $A_{db}(\lambda)$, there is no simple analytical solution for the reverse process,

https://doi.org/10.1021/acs.analchem.2c02037
Anal. Chem. 2022, 94, 11610−11618

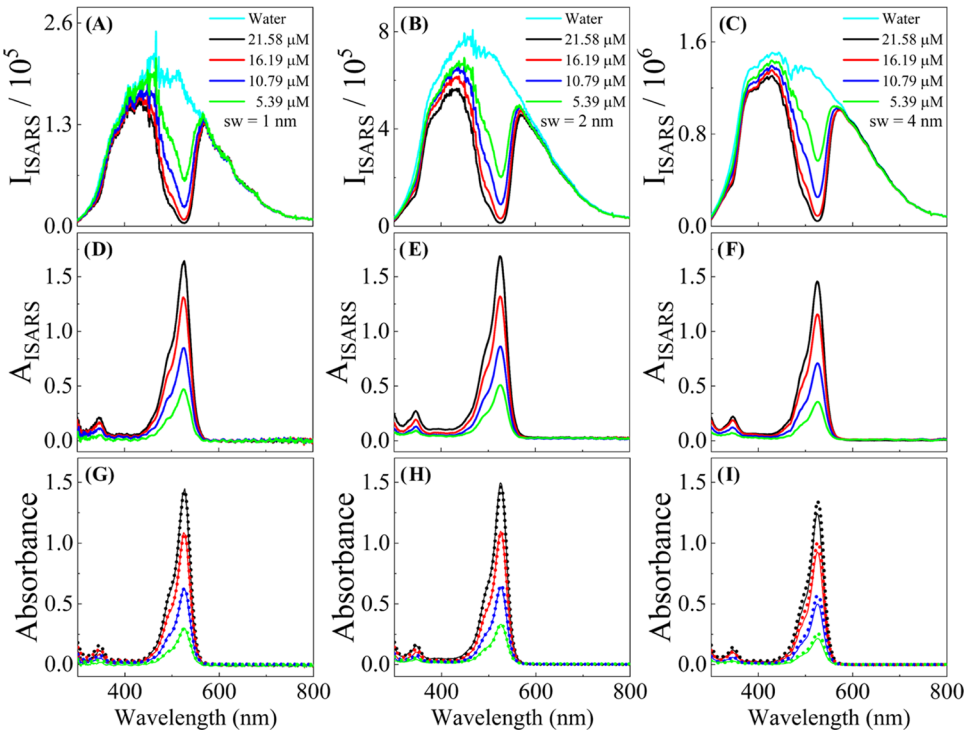

Figure 4. (A−C) Baseline-corrected ISARS spectra of the solvent and R6G at different concentrations with slit widths of 1, 2, and 4 nm, respectively. (D−F) ISARS UV−vis absorbance spectra that were calculated using the ISARS spectra shown in panels (A−C). (G−I) Head-to-head comparison of the (dash line) measured and (solid lines) deduced double-beam UV−vis absorbance spectra from the ISARS UV−vis spectra.

determination of the sample double-beam $A_{db}(\lambda)$ from its experimental $A_{ISARS}(\lambda)$. Fruitfully, this problem can be solved through the simple polynomial fitting of the numerical correlation between $A_{ISARS}(\lambda)$ and $A_{db}(\lambda)$, derived with the analytical model (eq 12), and using the experimental $A_s(\lambda)$, $r(\lambda)$, and $f(\lambda)$ values evaluated for each ISARS wavelength. A third polynomial with a general form of eq 13 gives an excellent fitting using the experimental $A_s(\lambda)$, $r(\lambda)$, and $f(\lambda)$ values obtained for individual ISARS wavelengths. An example of such a third polynomial fitting is shown in Figure 3F using the data generated with eq 12 and the $A_s(\lambda)$, $r(\lambda)$, and $f(\lambda)$ values obtained in Figure 3D. Since $A_s(\lambda)$, $r(\lambda)$, and $f(\lambda)$ values are available for every ISARS wavelength (Figure S5), a wavelength-specific third-order polynomial is available across the UV−vis wavelength region for wavelength-by-wavelength conversion of the sample ISARS-based absorbance to its double-beam absorbance. For discussion simplicity, we refer to $A_{db}^{ISARS}(\lambda)$ as the double-beam UV−vis absorbance deduced from the experimental $A_{ISARS}(\lambda)$ spectrum and to also differentiate the deduced double-beam absorbance $A_{db}^{ISARS}(\lambda)$ from $A_{db}(\lambda)$, the UV−vis absorbance directly measured with double-beam spectrophotometer.

$$A_{db}^{ISARS}(\lambda) = a_3(\lambda)(A_{ISARS}(\lambda))^3 + a_2(\lambda)(A_{ISARS}(\lambda))^2 + a_1(\lambda)A_{ISARS}(\lambda) + a_0(\lambda) \quad (13)$$

The effectiveness of eq 13 for predicting the sample double-beam UV−vis absorbance from its ISARS-based absorbance is investigated with R6G (Figure 4). Since R6G has not been used for the quantification of $A_s(\lambda)$, $r(\lambda)$, and $f(\lambda)$ values at any ISARS wavelengths, it allows the critical validation of third-order polynomial equations derived from these values. Further, as an ORF-active molecular fluorophore, R6G is approximately a pure absorber in the wavelength region below 515 nm under resonance excitation and detection conditions, but it is a simultaneously light absorber and emitter in its ORF-active region from 515 to 560 nm.[21] As such, R6G allows us to explore not only the effectiveness of converting the sample ISARS-based absorbance to its double-beam absorbance but also the possible ORF interference on the ISARS-based absorbance quantification. The reason we use R6G with a relatively broad absorbance range (~0.25−1.5) is to probe the possible concentration dependence of this ISARS-based double-beam absorbance quantification method.

The R6G ISARS intensity monotonically increases with increasing monochromator bandwidth (Figure 4A−C), which is due to the amount of incident and detected photons both increasing with increasing slit widths. However, the $A_{ISARS}(\lambda)$ (Figure 4D,E) and $A_{db}^{ISARS}(\lambda)$ (Figure 4G,H) obtained with the 1 nm slit width are essentially identical to their respective counterpart acquired with 2 nm slit widths. Furthermore, the $A_{db}^{ISARS}(\lambda)$ and $A_{db}(\lambda)$ obtained with the 1 and 2 nm slit widths are all in excellent agreement across the entire wavelength region, regardless of the R6G ORF activity at the specific wavelength and the R6G concentrations. These observations offer a critical validation of the ISARS method for predicting the sample double-beam absorbance and demonstrated the robustness of the ISARS technique against the fluorescence interference on the $A_{ISARS}(\lambda)$ or $A_{db}^{ISARS}(\lambda)$ evaluation. Otherwise, the R6G $A_{db}^{ISARS}(\lambda)$ intensity will be lower than $A_{db}(\lambda)$ in its ORF-active wavelength region from 515 to 565 nm.[21]

The R6G absorbance quantified with the commercial IS-equipped spectrophotometer (Shimadzu UV-2600i, integrating-sphere accessory ISR-2600) is significantly lower than that obtained with the same spectrophotometer with no IS, while the $KMnO_4$ absorbance spectrum acquired with the IS-

https://doi.org/10.1021/acs.analchem.2c02037
Anal. Chem. 2022, 94, 11610−11618

equipped UV−vis spectrophotometer is essentially the same as that obtained without the IS (Figure S8). This data confirms that the IS-based absorbance quantification with a UV−vis spectrophotometer as the detector is susceptible to fluorescence interference, as discussed in the Introduction section. Collectively, the R6G data shown in Figures 4 and S8 provides conclusive evidence that ISARS is drastically more reliable than the IS-equipped spectrophotometers for quantifying the light absorbance of fluorescent samples.

The peak intensities of $A_{db}(\lambda)$, $A_{ISARS}(\lambda)$, and $A_{db}^{ISARS}(\lambda)$ spectra obtained with a monochromator bandwidth of 4 nm are significantly smaller than their respective counterparts obtained with 1 and 2 nm, which is due to the polychromatic effect in the absorbance measurements.[40] The UV−vis absorbance reduces when the monochromator bandwidth for the spectral acquisition is broader than the intrinsic peak wavelengths where the spectral intensity is approximately constant. One possible reason the $A_{db}^{ISARS}(\lambda)$ intensity obtained with the 4 nm monochromator bandwidth is lower than that of the $A_{db}(\lambda)$ (Figure 4I) that is also acquired with 4 nm bandwidth is the mismatch between the monochromator used for the spectrophotometer-based $A_{db}(\lambda)$ measurements and spectrofluorometer-based $A_{db}^{ISARS}(\lambda)$ measurements.

Mechanistically, the absence of significant ORF interference on the ISARS-based absorbance quantification in the sample ORF-active wavelength region is due to the relatively low sample ORF quantum yield, which is usually below 0.03 for common molecular fluorophores[21] and the fact that ORF photons inside the IS can be reabsorbed by the sample or the IS itself. The reabsorbed ORF photons will either be converted to heat or re-emit as secondary fluorescence photons. However, the probability of the remitted fluorescence remaining in the narrow (1−4 nm) resonance excitation and emission wavelength regions should be very small.

While the small monochromator bandwidth is more robust against ORF interferences, the large monochromator bandwidth offers a higher spectral signal-to-noise ratio. All our subsequent ISARS-based spectral acquisition is performed with a monochromator bandwidth of 2 nm since this monochromator bandwidth offers a higher spectral signal-to-noise ratio without introducing spectral distortion.

Nanoparticle Absorption and Scattering Extinction. The utility of the ISARS technique for experiment quantification of the absorption and scattering extinction contribution to the sample UV−vis extinction measured with a double-beam spectrophotometer is demonstrated with three representative nanomaterials PSNP, fPSNP, and QD. PSNPs have been assumed to be pure light scatters in the wavelength region from 300 to 800 nm.[19,21,41] The optical properties of QDs and fPSNP are much more complicated. Under resonance excitation and detection conditions, QDs and fPSNP are simultaneous light absorbers, scatterers, and emitters in the wavelength region where the sample fluorescence excitation and emission spectra overlap but are simultaneous light scatterers and absorbers or pure scatterers in the other wavelength regions.[16,21] Regardless of their differences, none of the UV−vis spectra obtained with these samples using the double-beam spectrophotometer can be interpreted as the sample absorbance spectrum.

The first step for ISARS quantification of the sample absorption and scattering contribution to its double-beam extinction spectrum is to deduce the sample double-beam absorbance spectrum through the ISARS measurement (Figure 5A,C,E). The scattering extinction spectrum is then obtained by subtracting the double-beam absorbance from the sample

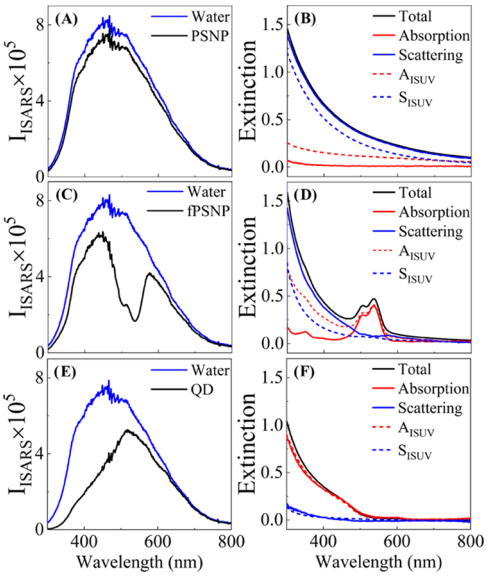

Figure 5. (A, C, E) Baselined-corrected ISARS spectra of solvent water and specified nanoparticle. Comparison of the total extinction spectrum, ISARS-derived double-beam absorption and scattering extinction spectra, and ISUV-derived absorption and scattering spectra obtained with (B) PSNP, (D) fPSNP, and (F) QD.

double-beam UV−vis extinction spectrum (eq 14). Conversely, light scattering extinction based on measurements performed with the IS-equipped UV−vis spectrophotometer is obtained by subtracting $A_{ISUV}(\lambda)$ spectra from the double-beam UV−vis extinction spectrum (eq 15).

$$S_{db}^{ISARS}(\lambda) = E_{db}(\lambda) - A_{db}^{ISARS}(\lambda) \quad (14)$$

$$S_{ISUV}(\lambda) = E_{db}(\lambda) - A_{ISUV}(\lambda) \quad (15)$$

The ISARS data shows that the relative absorption and scattering contribution to the nanomaterials' UV−vis extinction spectra vary significantly from one type of nanoparticles to another. A PSNP of 380 nm in diameter (Figure 5A,B) is predominantly light scattered across the entire wavelength region from 300 to 800 nm. The highest absorbance contribution to the PSNP UV-extinction is less than 5%, which is observed at 300 nm. In contrast, QD (Figure 5E,F) is predominantly a light absorber in the wavelength region with detectable UV−vis features (<620 nm), while the relative light scattering and absorption contribution to the fPSNP extinction spectrum (Figure 5C,D) are highly wavelength-dependent. The double-beam absorbance spectrum $A_{db}^{ISARS}(\lambda)$ determined from the fPSNP ISARS measurement qualitatively resembles a UV−vis spectrum of organic dye. Unfortunately, it is impossible to compare the $A_{db}^{ISARS}(\lambda)$ acquired with fPSNP with that obtained with the free dye in solution because the fPSNP composition is vendor's propriety information. Nonetheless, the fact that the ISARS-derived fPSNP scattering extinction spectrum resembles the general shape of PSNP scattering extinction spectrum provides strong supporting evidence of the accuracy of this ISARS methodology. Overall, the data obtained with the three representative nanoparticles that differ significantly in their relative scattering and absorption activities shows the effectiveness of the ISARS

https://doi.org/10.1021/acs.analchem.2c02037
Anal. Chem. 2022, 94, 11610−11618

methodology for the experimental separation of the sample UV−vis extinction spectra measured with double-beam spectrophotometer into its absorption and scattering extinction spectra.

While the R6G data (Figure S8) showed the susceptibility of the IS-equipped spectrophotometer to fluorescence interference in fluorescence quantification, the data obtained with the PSNP and fPSNP (Figure 5) demonstrated the susceptibility of this technique to the light scattering interferences. Polystyrene is a known light scatterer and has been commonly used for light scattering-based sizing, and the ISARS method showed that there is no significant PSNP light absorption across the entire wavelength region. However, the IS-equipped spectrophotometer gives falsely high UV−vis absorbance in the entire wavelength. The reason that the broad-band absorbance in the A_{ISUV} spectrum of fPSNP is higher than that of PSNP is most likely due to their different sizes. fPSNPs are about 10 nm in diameter and can be approximated as Rayleigh scatterers with the probed wavelength ranges. In this case, the scattered photons propagated globally from every direction; only the scattered photons that propagated forward can be captured by the IS. The large amount of the scattered photon that escapes the IS capture lead to significantly overestimated sample absorbance. In contrast, the PSNPs are about 380 nm in diameter and are likely Mie scatterers. This means that the scattered light is predominantly being propagated in the forward and backward directions. In this case, the fraction of the scattered photons escaping the IS capture is relatively small. Therefore, the degree of the absorbance overestimation for PSNPs is small in comparison to that for fPSNPs.

CONCLUSIONS

We developed an ISARS spectroscopic method and demonstrated its utility for quantification of the double-beam UV−vis absorbance spectra for samples with different optical complexities, from approximately pure light absorbers, pure scatterers, to simultaneous absorbers, scatterers, and emitters. A nonlinear three-parameter analytical model was developed for correlating the sample ISARS-based and double-beam UV−vis absorbance. Theoretical background and experimental methods for the ISARS baseline correction and ISRAS-based absorbance quantification are provided. The optimal excitation and detection wavelength bandwidth for the ISARS acquisition is 2 nm, as it offers a high spectral signal-to-noise ratio without causing detectable spectral distortion. This ISARS-based UV−vis absorbance quantification method can be implemented by any researcher with access to spectrofluorometers coupled with an integrating-sphere accessory. It is applicable to all solution samples for the quantitative separation of light absorption and scattering contribution to the sample UV−vis extinction spectra obtained with a conventional double-beam spectrophotometer. We believe that with its broad accessibility and applicability, this ISARS method will evolve as a popular technique for characterizing emerging macromolecules, supramolecules, and nanoscale materials that are often simultaneous light absorbers, scatterers, and some cases also emitters.

ASSOCIATED CONTENT

Supporting Information

The Supporting Information is available free of charge at https://pubs.acs.org/doi/10.1021/acs.analchem.2c02037.

Derivation of eqs 3−5; baseline spectra obtained with $NiSO_4$; effective sample volume on baseline quantification; correlations between $NiSO_4$ $A_{db}(\lambda)$ and $A_{ISARS}(\lambda)$; solvent and barium sulfate fluorescence spectrum; and UV−vis and ISUV spectra of R6G and $KMnO_4$ absorbance spectra (PDF)

AUTHOR INFORMATION

Corresponding Author

Dongmao Zhang − *Department of Chemistry, Mississippi State University, Mississippi State, Mississippi 39762, United States;* orcid.org/0000-0002-2303-7338; Email: Dongmao@chemistry.msstate.edu

Authors

Max Wamsley − *Department of Chemistry, Mississippi State University, Mississippi State, Mississippi 39762, United States;* orcid.org/0000-0001-6790-4846

Pathum Wathudura − *Department of Chemistry, Mississippi State University, Mississippi State, Mississippi 39762, United States*

Juan Hu − *Department of Mathematical Sciences, DePaul University, Chicago, Illinois 60604, United States*

Complete contact information is available at: https://pubs.acs.org/10.1021/acs.analchem.2c02037

Author Contributions

[§]M.W. and P.W. contributed equally to this work.

Notes

The authors declare no competing financial interest.

ACKNOWLEDGMENTS

This work was supported in part by the Center of Biomedical Research Excellence Program funded through the Center for Research Capacity Building in the National Institute for General Medical Sciences (P20GM103646), and by an NSF Grant (CHE 2203571). The content is solely the responsibility of the authors and does not necessarily represent the official views of the National Institutes of Health or National Science Foundation.

REFERENCES

(1) Westmoreland, D. E.; López-Arteaga, R.; Kantt, L. P.; Wasielewski, M. R.; Weiss, E. A. *J. Am. Chem. Soc.* **2022**, *144*, 4300−4304.

(2) Curcio, A.; Van de Walle, A.; Benassai, E.; Serrano, A.; Luciani, N.; Menguy, N.; Manshian, B. B.; Sargsian, A.; Stefaan, S.; Espinosa, A.; et al. *ACS Nano* **2021**, *15*, 9782−9795.

(3) Wang, Y.; Shi, L.; Ma, D.; Xu, S.; Wu, W.; Xu, L.; Panahandeh-Fard, M.; Zhu, X.; Wang, B.; Liu, B. *ACS Nano* **2020**, *14*, 13056−13068.

(4) Luo, X.-M.; Gong, C.-H.; Pan, F.; Si, Y.; Yuan, J.-W.; Asad, M.; Dong, X.-Y.; Zang, S.-Q.; Mak, T. C. W. *Nat. Commun.* **2022**, *13*, No. 1177.

(5) Ruan, J.; Liu, H.; Chen, B.; Wang, F.; Wang, W.; Zha, Z.; Qian, H.; Miao, Z.; Sun, J.; Tian, T.; et al. *ACS Nano* **2021**, *15*, 11428−11440.

(6) Pan, Y.; Ma, X.; Liu, C.; Xing, J.; Zhou, S.; Parshad, B.; Schwerdtle, T.; Li, W.; Wu, A.; Haag, R. *ACS Nano* **2021**, *15*, 15069−15084.

(7) Popa, S.; Milea, M. S.; Boran, S.; Nitu, S. V.; Moşoarcă, G. E.; Vancea, C.; Lazău, R. I. *Sci. Rep.* **2020**, *10*, No. 16100.

(8) Shi, X.; Dai, C.; Wang, X.; Hu, J.; Zhang, J.; Zheng, L.; Mao, L.; Zheng, H.; Zhu, M. *Nat. Commun.* **2022**, *13*, No. 1287.

(9) Pignataro, M. F.; Herrera, M. G.; Dodero, V. I. *Molecules* **2020**, *25*, 4854.
(10) Xu, J. X.; Niu, G.; Tang, B. Z.; Zhang, D. *J. Mater. Chem. C* **2019**, *7*, 12086−12094.
(11) Zhao, Y.; Hu, Y.; Zhong, Y.; Wang, J.; Liu, Z.; Bai, F.; Zhang, D. *J. Phys. Chem. C* **2021**, *125*, 22318−22327.
(12) Baskar, A. V.; Benzigar, M. R.; Talapaneni, S. N.; Singh, G.; Karakoti, A. S.; Yi, J.; Al-Muhtaseb, A. aH.; Ariga, K.; Ajayan, P. M.; Vinu, A. *Adv. Funct. Mater.* **2022**, *32*, No. 2106924.
(13) Dong, H.; Sun, L.-D.; Yan, C.-H. *J. Am. Chem. Soc.* **2021**, *143*, 20546−20561.
(14) Zhang, C.; Chen, W.; Zhang, T.; Jiang, X.; Hu, Y. *J. Mater. Chem. B* **2020**, *8*, 4726−4737.
(15) Wy, Y.; Jung, H.; Hong, J. W.; Han, S. W. *Acc. Chem. Res.* **2022**, *55*, 831−845.
(16) Xu, J. X.; Vithanage, B. C. N.; Athukorale, S. A.; Zhang, D. *Analyst* **2018**, *143*, 3382−3389.
(17) Collings, P. J.; Gibbs, E. J.; Starr, T. E.; Vafek, O.; Yee, C.; Pomerance, L. A.; Pasternack, R. F. *J. Phys. Chem. B* **1999**, *103*, 8474−8481.
(18) Liu, B.-J.; Lin, K.-Q.; Hu, S.; Wang, X.; Lei, Z.-C.; Lin, H.-X.; Ren, B. *Anal. Chem.* **2015**, *87*, 1058−1065.
(19) Xu, J. X.; Yuan, Y.; Zou, S.; Chen, O.; Zhang, D. *Anal. Chem.* **2019**, *91*, 8540−8548.
(20) Xu, J. X.; Hu, J.; Zhang, D. *Anal. Chem.* **2018**, *90*, 7406−7414.
(21) Siriwardana, K.; Vithanage, B. C. N.; Zou, S.; Zhang, D. *Anal. Chem.* **2017**, *89*, 6686−6694.
(22) Gaigalas, A. K.; He, H.-J.; Wang, L. *J. Res. Natl. Inst. Stand. Technol.* **2009**, *114*, 69−81.
(23) Mann, S. A.; Sciacca, B.; Zhang, Y.; Wang, J.; Kontoleta, E.; Liu, H.; Garnett, E. C. *ACS Nano* **2017**, *11*, 1412−1418.
(24) Mori, A.; Yamashita, K.; Tabata, Y.; Seto, K.; Tokunaga, E. *Rev. Sci. Instrum.* **2021**, *92*, No. 123103.
(25) Nelson, N. B.; Prézelin, B. B. *Appl. Opt.* **1993**, *32*, 6710−6717.
(26) Butler, W. L. *J. Opt. Soc. Am.* **1962**, *52*, 292−299.
(27) Sun, L.; Bolton, J. R. *J. Phys. Chem. A* **1996**, *100*, 4127−4134.
(28) Tassan, S.; Ferrari, G. M. *Appl. Opt.* **2003**, *42*, 4802−4810.
(29) Edwards, D. K.; Gier, J. T.; Nelson, K. E.; Roddick, R. D. *J. Opt. Soc. Am.* **1961**, *51*, 1279−1288.
(30) Gaigalas, A. K.; Wang, L.; Karpiak, V.; Zhang, Y. Z.; Choquette, S. *J. Res. Natl. Inst. Stand. Technol.* **2012**, *117*, 202−215.
(31) Gaigalas, A. K.; Wang, L.; Choquette, S. *J. Res. Natl. Inst. Stand. Technol.* **2013**, *118*, 1−14.
(32) Roos, A. *Appl. Opt.* **1991**, *30*, 468−474.
(33) Nilsson, A. M. K.; Berg, R.; Andersson-Engels, S. *Appl. Opt.* **1995**, *34*, 4609−4619.
(34) Würth, C.; Lochmann, C.; Spieles, M.; Pauli, J.; Hoffmann, K.; Schüttrigkeit, T.; Franzl, T.; Resch-Genger, U. *Appl. Spectrosc.* **2010**, *64*, 733−741.
(35) Pålsson, L. O.; Monkman, A. P. *Adv. Mater.* **2002**, *14*, 757−758.
(36) Würth, C.; Grabolle, M.; Pauli, J.; Spieles, M.; Resch-Genger, U. *Nat. Protoc.* **2013**, *8*, 1535−1550.
(37) Brouwer, A. M. *Pure Appl. Chem.* **2011**, *83*, 2213−2228.
(38) Zhang, W.; Zilevu, D.; Creutz, S. E.; Zhang, D. *J. Phys. Chem. C* **2020**, *124*, 20388−20397.
(39) Xu, J. X.; Yuan, Y.; Liu, M.; Zou, S.; Chen, O.; Zhang, D. *Anal. Chem.* **2020**, *92*, 5346−5353.
(40) Skoog, D. A.; Holler, F. J.; Crouch, S. R. *Principles of Instrumental Analysis*, 7th ed.; Thomson Brooks/Cole: Belmont, CA, 2007.
(41) Xu, J. X.; Siriwardana, K.; Zhou, Y.; Zou, S.; Zhang, D. *Anal. Chem.* **2018**, *90*, 785−793.

https://doi.org/10.1021/acs.analchem.2c02037
Anal. Chem. 2022, 94, 11610−11618